Electrochimica Acta 508 (2024) 145273

Contents lists available at ScienceDirect

Electrochimica Acta

journal homepage: www.journals.elsevier.com/electrochimica-acta

Effect of high-boiling point solvents on inkjet printing of catalyst layers for proton exchange membrane fuel cells

Qingying Zhao [a,b], Tobias Morawietz [a], Pawel Gazdzicki [a], K. Andreas Friedrich [a,b,*]

[a] German Aerospace Center (DLR), Institute of Engineering Thermodynamics, Pfaffenwaldring 38-40, 70569, Stuttgart, Germany
[b] University of Stuttgart, Institute of Building Energetics, Thermal Engineering and Energy Storage (IGTE), Pfaffenwaldring 31, 70569, Stuttgart, Germany

ARTICLE INFO

Keywords:
High boiling point solvents
Ink formulation
Inkjet-printed catalyst layers
Solvent effect
Proton exchange membrane fuel cell

ABSTRACT

Inkjet printing (IJP) is considered as a promising and flexible method for low cost and drop-on-demand pattern formation in proton exchange membrane (PEM) fuel cells. Although significant advancements have been made in inkjet-printed electrodes, identifying the optimal ink formulations remains challenging due to severe restrictions on the ink properties. Generally, the catalyst layer prepared by IJP using low boiling point solvents (water/alcohol) show reasonable electrochemical performance. However, low boiling point solvents lead to clogging of the printhead nozzle due to fast evaporation of the solvent in the inkjet print head. In this study, high boiling point solvents (propylene glycol (PG) or ethylene glycol (EG)) were used as additives to reduce nozzle clogging and improve printing efficiency. In this context, the relationship between catalyst ink properties, CL microstructure, and electrochemical performance of the MEA is investigated. Results show that printing time is significantly reduced with adding high boiling point solvents in the ink (66.67% reduction of time with 30 wt% PG). However, an increased amount of additive is detrimental in terms of electrochemical performance due to formation of larger agglomerates, lower porosity of the catalyst layer, and reduced ECSA. The results of this work can be used to develop a strategy to adjust the trade-off between printing time and electrochemical performance of electrodes prepared using IJP.

1. Introduction

PEM fuel cells are a promising technology for emission free energy conversion based on clean hydrogen as fuel. They have broad application prospects in stationary area and electrification of transportation [1], particularly in long-distance heavy-duty applications. Currently, there have been significant advancements in the performance of membrane electrode assembly (MEA) components. Studies showed that MEA are commonly fabricated by slot-die [2], ultrasonic spray [3], air-spray [4] and screen printing [5], and the coating technique can have great impact on the resulting catalyst layer [6]. Inkjet printing (IJP) has been applied as a novel fabrication method for printing electrode in PEM fuel cells as well [7,8]. It offers various advantages such as the facile process, versatile pattern, and precise deposition of minute amounts of materials. However, this promising method is not yet established as mass manufacturing technique in the PEM fuel cell area due to the relatively low fabrication efficiency compared with current technique like roll-to-roll coating. Furthermore, inkjet printing technology can lead to a cost advantage compared with traditional preparation methods in reducing waste of Pt catalyst, which comprises 41% of the whole stack cost based on 500,000 fuel cell systems produced per year [9]. The inkjet printing technology allows for precise control of material usage by depositing catalyst inks only where it is needed.

Up to now, great efforts have been made to study the influence of solvent types on the performance of MEA and high volatility solvents especially alcohol and water [10] are the most common choices. For example, Ren et al. [11] suggested water/IPA mixture solvents with 50 wt% alcohol content during the spray process, ensuring satisfactory fuel cell performance due to its proper ionomer and pore size distribution. Gong et al., [12] applied the solvent composition (n-PA/H_2O mixtures) and a catalyst ink containing 90 wt% H_2O is preferred during the ultrasonic spraying, leading optimal MEA performance. However, the selection of dispersants used in the typical ink should be tailored to the type of fabrication process [13]. Inkjet printing requires inks with low volatility/high viscosity to enable efficient jetting through the micrometer-sized nozzles [14]. High volatility/low viscosity results in a smaller volume of a single droplet, leading to the necessity of printing more layers to achieve a certain platinum loading. In addition, the

* Corresponding author.
E-mail address: Andreas.Friedrich@dlr.de (K.A. Friedrich).

https://doi.org/10.1016/j.electacta.2024.145273
Received 29 July 2024; Received in revised form 21 October 2024; Accepted 21 October 2024
Available online 22 October 2024

combination of alcohol/water is highly volatile, and the nozzle can be easily clogged after jetting drops. It is apparent that ink properties are the most crucial aspect of inkjet printing of catalyst layers. Shukla et al., [15] employed a mixture of PG and IPA for inkjet printing technique, where PG proportion exceeds 30 wt%. Unfortunately, high concentration of a high-boiling-point solvent causes cracks on the CL printed over membrane, which should be avoided due to the adverse effect on performance [16] and durability [17].

Our work aims at characterizing electrodes prepared by inkjet printing with a Pt loading of around 0.1 mg cm^{-2} at the anode and the cathode, respectively. This work aims to investigate the effect of additive concentration on MEA structure and performance to allow optimization of inkjet-printed electrodes. Specifically, the effects of the solvent composition on the dispersion of catalyst and ionomer particles, and the microstructure of catalyst layers were investigated in detail. Distribution of diluted ink was analyzed by transmission electron microscopy (TEM) and dynamic light scattering (DLS). Analyses of printed ink drops were performed using atomic force microscopy (AFM). The transport of liquid water within the catalyst layer is influenced by the microstructure of the CL and the degree of hydrophobicity [18]. Thus, the analysis of the microstructure of the CL was carried out at cross-sections by focused ion beam scanning electron microscopy (FIB-SEM) and scanning electron microscope (SEM). Hydrophobicity was studied by average static contact angle. Finally, the MEA performance and electrochemical properties were investigated using IV-characteristics, cyclic voltammetry (CV) and electrochemical impedance spectroscopy (EIS).

2. Experimental method

2.1. Ink preparation and MEA fabrication

The catalyst inks were prepared by mixing commercial 40 wt% Pt/C catalyst (Hispec 4000, Alfa chemistry), Nafion ionomer solution (Nafion® 117 solution), and mixture solvents. As shown in Fig. 1, the IPA/H_2O was added to the Pt/C catalyst firstly, followed by propylene glycol (PG) or ethylene glycol (EG) additives in varying mass percentage concentration and Nafion solution with a weight ratio of ionomer to carbon (I/C) of 0.8 to prepare the ink required for printing. Ink without PG or EG was also prepared for comparison as standard ink. A set of five catalyst inks were formulated with 5 wt% PG, 10 wt% PG, 30 wt% PG, 5 wt% EG, and 0 wt% additive (PG or EG) as shown in Table S1 for details. Then, inks were dispersed by sonication for 30 min in ice water to be homogenous. All inks were inkjet printed by Dimatix Materials Printer DMP-2850 (Fujifilm) with 10 picolitre cartridge. The printhead consists of 16 nozzles linearly spaced at the distance of 254 μm and each nozzle opening has a diameter of 20 μm. Nafion HP membranes and aluminum foil were placed side by side on the printing table and a CL was printed on both substrates, ensuring the same loading and the same active area of 3.6 cm^2 (4.5 cm x 0.8 cm) for both layers. The CL printed on the aluminum foil were used to determine the Pt loading by gravimetric method. The coated membranes were dried in a vacuum oven at 60 °C for 3 h. Differently, the aluminum foils coated with CL were dried at 150 °C for 3 h in a vacuum oven after the inkjet printing progress. The Pt loading of the CL was determined by weighing the aluminum foils before and after the inkjet printing progress to calculate an average mass of CL. For both catalyst layers at anode and cathode, the Pt loading was controlled to be (0.10 ± 0.03) mg cm^{-2}. The uncertainty of the Pt loading corresponds to reproducibility of the printed CL (5 samples). The prepared catalyst-coated membranes (CCMs) were sandwiched between gas diffusion layers (GDLs, SGL 25BC, SIGRACET®, SGL Group) with an active area of 3.6 cm^2 without hot pressing.

3. Physical characterizations

3.1. Characterization of the particle distribution in the diluted ink and morphology of printed drops and CLs

The particle distribution was measured by Zetasizer Ultra (Malvern Panalytical Ltd) to evaluate the ink dispersion. The distributions were evaluated by using diluted ink, which was prepared by adding 10 μL ink to 5 mL corresponding mixture solvents described in ink preparation. Above diluted ink was also characterized by S/TEM at core facility SRF AMICA (Stuttgart Research Focus Advanced Materials Innovation and Characterization) at the University of Stuttgart. TEM imaging was performed on Spectra 300 microscope (ThermoFisher, USA) at the electron accelerating voltage of 300 kV for the morphology and structure of the catalyst-ionomer agglomerates. Examination of the surface morphologies of CLs was performed by SEM (Zeiss Crossbeam 350), which was operated at an accelerating voltage of 2 kV with an Everhart-Thornley secondary electron (SE) detector for imaging. The fresh CLs were cut by FIB-SEM (Zeiss Crossbeam 350) at 30 kV and 700 pA after preparing the trenches with higher currents. The imaging at the sectioned interface was performed at an acceleration voltage of 5 kV for the structural analysis. Additionally, surface morphologies of the inkjet-printed drops and catalyst layers were measured by AFM using an Icon XR (Bruker, Karlsruhe, Germany) with Nanoscope 6 controller. NanoScope Analysis 3.0 was employed to analyze samples characterized by AFM.

3.2. Contact angle measurement

Contact angle measurements were carried out using a homemade optical camera setup. A water drop of about 15 μL was deposited on the target CL surface. Pictures were then taken to capture the contact between the water droplet and the CL. The images were subsequently analyzed using ImageJ and its contact angle analysis plugin. An average value was calculated based on three measurements of each sample on different positions.

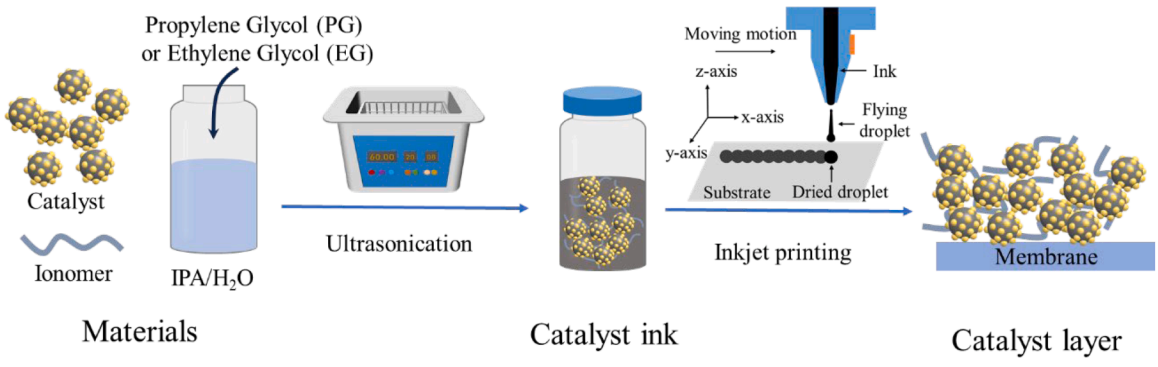

Fig. 1. Schematic diagram of the ink formulation and catalyst layer preparation.

3.3. Electrode porosity

The total CL porosity (ϵ_V) can be assessed by ink compositions, thickness of catalyst layer and Pt loading, and determined by following equations [19,20]:

$$\epsilon_S = \frac{m_{Pt}}{L}\left(\frac{1}{\rho_{Pt}} + \frac{1 - Y_{Pt}}{Y_{Pt}\rho_c}\right) \quad (1)$$

$$\epsilon_N = \frac{m_{Pt}}{L}\frac{Y_{el}}{(1 - Y_{el})Y_{Pt}\rho_N} \quad (2)$$

$$\epsilon_V = 1 - (\epsilon_S + \epsilon_N) \quad (3)$$

Here, ϵ_S and ϵ_N presents for solid volume fraction and electrolyte volume fraction, respectively. m_{Pt} (g cm^{-2}) is the catalyst loading, L (μm) is the average thickness of catalyst layer collected from cross-sectional CLs by FIB-SEM, ρ_{Pt}, ρ_c and ρ_N are densities of Pt, carbon and Nafion, which are 21.5 g cm^{-3}, 2 g cm^{-3} and 1.9 g cm^{-3}, respectively. Y_{Pt} means the mass fraction of Pt on carbon support and Y_{el} is the Nafion loading on the cathode side.

3.4. Rheological measurements protocol

Rheological measurements were performed using a rheometer (MCR101, Anton Paar) with a stainless cone plate (50 mm diameter) at 25 °C. A pre-shear at 1 s^{-1} to 1,000 s^{-1} was applied before the formal measurements based on the published papers [21,22]. Considering the inkjet printing process imposes shear rates of the order of magnitude of 10^5–10^6 s^{-1} [23] and viscosity is stable when the shear rate is 100 s^{-1}, the steady-shear rheology measurements were finally conducted by increasing the shear rate from 1 s^{-1} to 1,000 s^{-1} and the area of 100 s^{-1} to 1,000 s^{-1} was chosen for the analysis.

3.5. Electrochemical characterization

The MEA was assembled using a homemade fuel cell hardware (5 × 5 cm^2) with 3-channel serpentine flow field and tested on homemade test bench [24]. However, the active area was limited to the air outlet region of the flow field by using a PTFE glass fabric film as a mask and the resulting actual flow field exhibited parallel channels and an active area of 3.6 cm^2 (4.5 × 0.8 cm^2) as shown in Fig. S1 in the supporting information. The break-in procedures were conducted according to the EU harmonized test protocols [25]. After break-in, polarization curves were recorded with an operating temperature of 80 °C under 1.5 bar (absolute pressure). Hydrogen and air, humidified to 50% or 80% relative humidity, were supplied to the anode and cathode side at fixed flow rates of 0.2 and 0.4 L min^{-1}, respectively. Under the same operating conditions, using a Zahner Zennium with PP241 potentiostat electrochemical impedance spectroscopy (EIS) measurements were conducted at 0.5 A cm^{-2} in a frequency range from 0.1 to 100,000 Hz with an AC perturbation amplitude of 5%. Cyclic voltammetry was recorded with a scan rate of 50 mV s^{-1} under ambient pressure at a cell temperature of 80 °C. Fully humidified H_2 and N_2 were both purged with 0.1 L min^{-1} at the anode and cathode, respectively. N_2 purging was carried out at the cathode side until the voltage dropped close to 0.1 V before CV measurement. Finally, ECSA values were determined using the electrochemical hydron desorption peaks by employing cyclic voltammetry between 0.1–1.2 V vs. RHE. The last cycle of six subsequent CV cycles was used. The proton transport resistance (R_{H+}) of CL was measured with a cell temperature of 80 °C and back pressure of 1.5 bar through in-situ EIS. H_2 and N_2 were supplied at the anode and cathode at the flow rate of 0.1/0.1 L min^{-1} with the humidity of 30%, 50% and 80%, respectively. Nyquist plots were recorded by Zahner Zennium with PP241 load at 0.4 V, with 10 mV AC amplitude from 100 kHz to 0.1 Hz. The proton transport resistance is determined by analyzing the recorded impedance spectra [26] and calculated by the method derived from Modestov et al. [27]. The length of the Warburg-like region projected onto the real impedance axis is equal to $R_{H+}/3$. The H_2 crossover current density was measured by chronoamperometry at 0.4 V under a gas flow of H_2/N_2 (0.1/0.1 L min^{-1}) and an RH of 100% at 80 °C. The average current density corresponds to the H_2 crossover current density.

4. Discussion and results

Inkjet-printed CLs in this study were fabricated using different inks, following the procedure depicted in Fig. 1. At the beginning of this section, the physical and electrochemical properties for CLs fabricated by different contents of PG are shown and analyzed in detail. The same type of investigation was carried out for CL made by ink with 5 wt% EG (CL-05E) and corresponding data are compared with results of CL made by ink with 5 wt% PG (CL-05P) in the second part.

Fig. 2 shows the number of printing layers and time to print CLs including nozzle cleaning for different ink using fixed I/C ratio. It should be noted that the time to print CLs including nozzle cleaning represents the entire process to produce a CCM after having the ink solution ready to use. Each nozzle cleaning takes 5–10 min depending on the clog severity, the print head to be disassembled and ultrasonication in ethanol. Cleanliness of the printhead was assessed by visual inspection. Without using high boiling point solvents, the nozzle requires to be cleaned every 3–4 printing layer of 3.6 cm^2, while cleaning is required only every 6–10 layer for inks with PG or EG additive, depending on additive concentration. Consequently, due to the addition of PG, the required time to fabricate an CL can be reduced up to 66.67% especially when the PG content increases to 30 wt%. At 5 wt% PG, the required time was reduced by 26.67%. However, there is substantial impact of the additives on physical properties of the CL and fuel cell performance which will be discussed in the following.

DLS study reveals the particle size distributions of the catalyst-ionomer and ionomers, which are presented in Fig. 3a and b. Fig. 3a shows similar size distributions for all samples, revealing similar hydrodynamic diameter of catalyst-ionomer in diluted ink. However, the morphology of the ionomers can be greatly affected by the solvent components in Fig. 3b. The size distribution shifts to right at the range of 100–1,000 nm, implying the average particle size of the ionomers prepared by ink with lower PG contents is smaller than that by ink containing higher PG contents. Thus, ionomers are less clustered in the ink at low PG content and thin ionomer layer can be formed on the catalyst interface with more homogeneous distribution. TEM was used to visualize the morphology and structure of the catalyst-ionomer agglomerates in the diluted ink [28] with different PG contents as shown in Figs. 3c–e and S2 in the supporting information. Figs. 3c and S2a–c (see

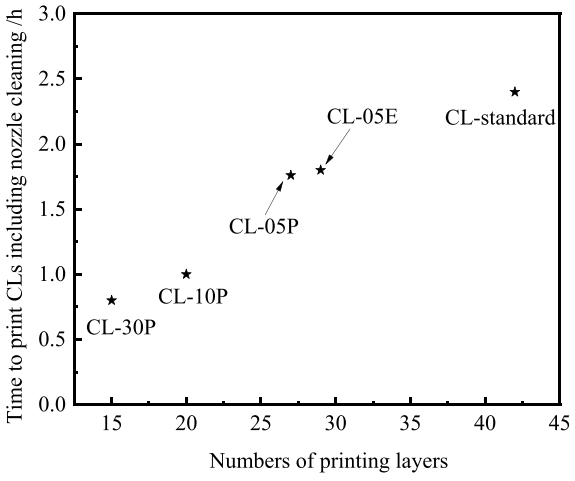

Fig. 2. The relationship of time to print CLs including nozzle cleaning and numbers of printing layers with Pt loading of ~ 0.1 mg cm^{-2} for different inks.

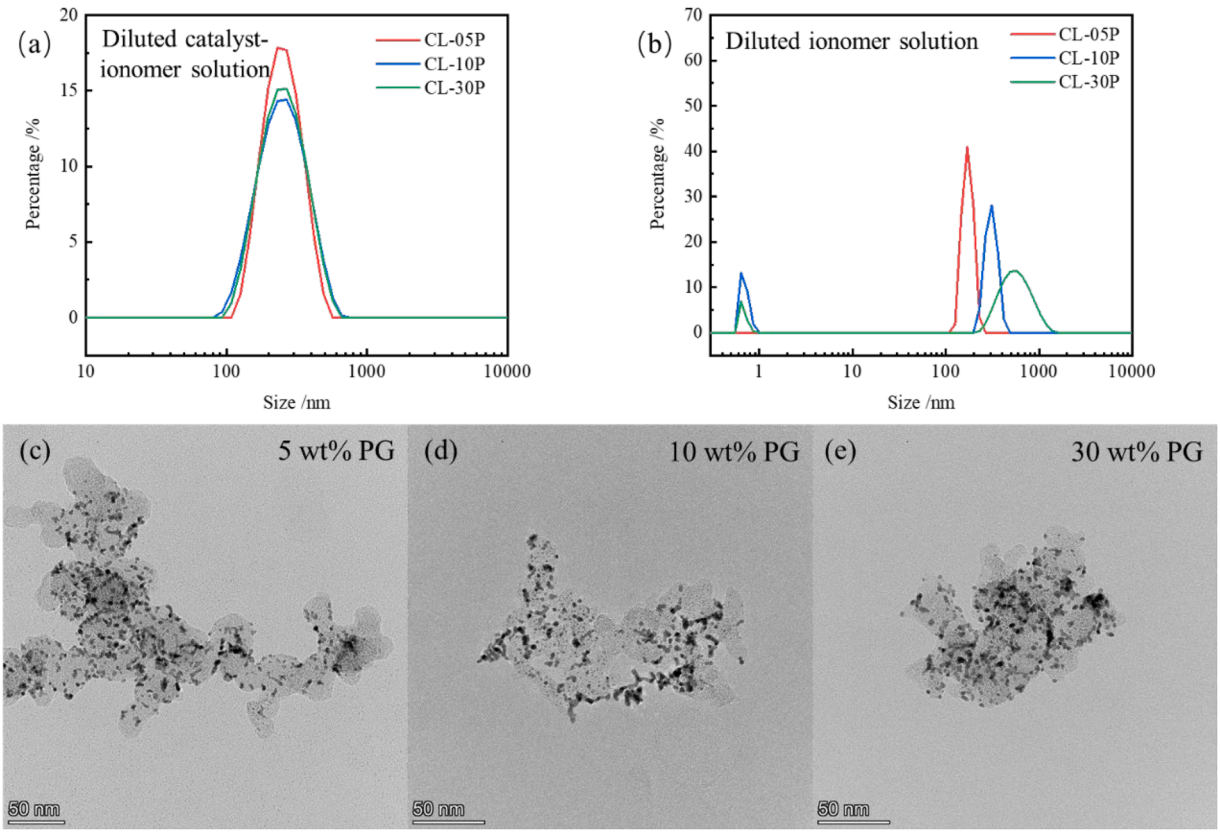

Fig. 3. DLS analysis of (a) diluted catalyst-ionomer solution and (b) diluted ionomer solution (without catalyst) with different PG contents. TEM images of (c-e) diluted ink containing different PG contents.

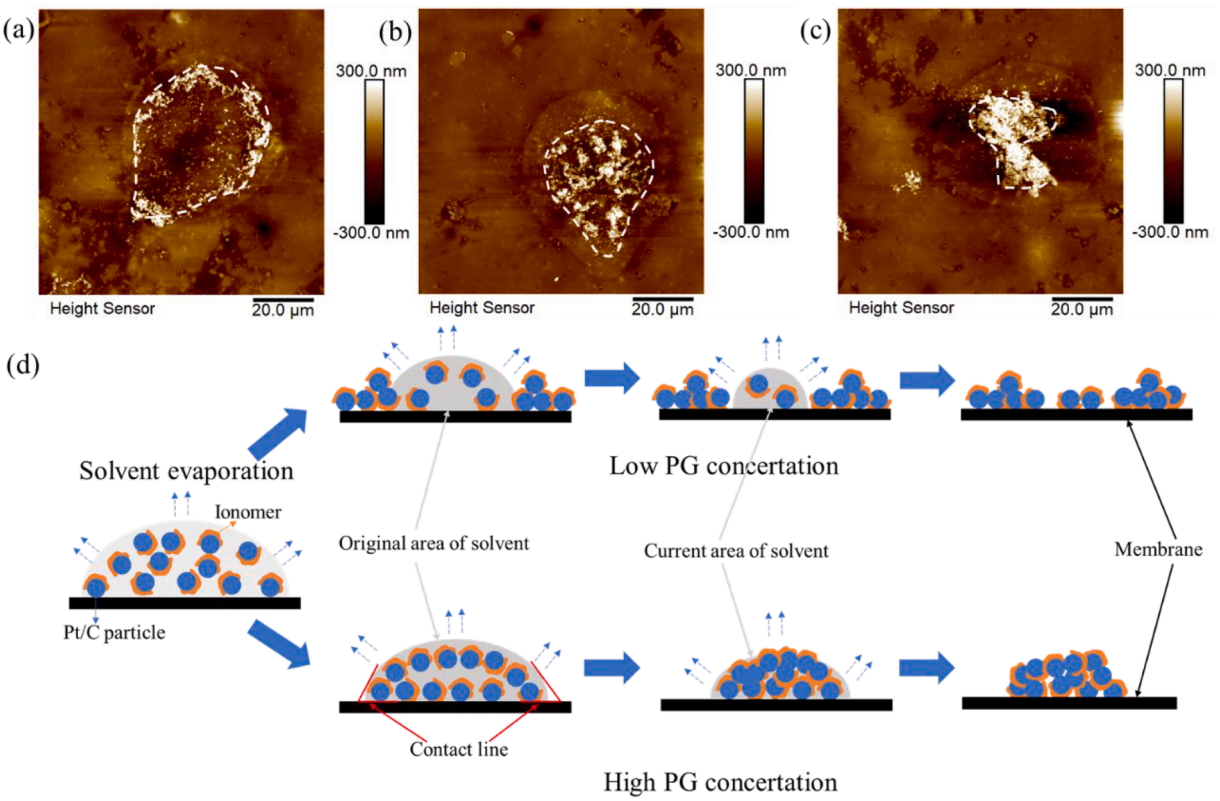

Fig. 4. AFM images of inkjet-printed individual droplets with varying ink concentration (a) 5 wt% PG, (b)10 wt% PG, and (c) 30 wt% PG; (d) Schematic diagram of the droplet evaporation during drying process. Bright gray means the original solvent interface before evaporation, and dark gray means the current solvent interface.

supporting information) showed lengthy agglomerates, implying weakened agglomeration behavior. A different morphology of agglomerates is observed at 10 wt% PG which is more compact and ellipsoidal (Figs. 3d and S2d–f in supporting information). This behavior is even stronger at 30 wt% PG (Figs. 3e and S2g–i in supporting information). Hence, the increase in the PG content seems to promote the largely aggregated free ionomers in Fig. 3b, a thick but narrowly confined ionomer layer adsorbed on the catalyst surface [29] and largely aggregated Pt/C-ionomer agglomerates [30] in Fig. 3e.

Drop formations on membrane after injection for ink containing different PG contents are shown in Figs. 4a–c and S3 (supporting information). It is mentioned that the viscosity of PG (39.44 cp) is much higher than that of water (0.89 cp) or isopropanol (2.07 cp), see Table S2. Therefore, the increasing concentration of PG additive results in an increase in the ink's viscosity (see Fig. S4, supporting information). In addition, the PG additive also influences the size and shape of the printed drops. As the PG content increases, the length of the flying droplet and velocity of the droplet decreases in Fig. S3e and f, (supporting information) leading to the Feret's Diameter [31] (calculated by open source software-ImageJ) of the irregular drop decreases from (62 ±6) μm to (57±6) μm and (47±8) μm based on Fig. S3b–d (supporting information). AFM analysis also reveals that PG content impacts the morphology of dried droplets. When the PG content is relatively low, the dried droplets are heterogeneous and exhibit coffee-ring effect, where particles mainly concentrated at the edge and a small number of catalyst-ionomer particles situated at the center. As the PG content increases, agglomerates tend to concentrate inward, leading to a decrease in drop size and more homogeneous particle distribution. It should be noted that quantification of ionomer distribution is not possible based on these images because ionomers in CL and Nafion substrate cannot be clearly distinguished due to same chemical composition. Fig. 4d shows a scheme of drop formation after printing considering evaporating conditions caused by inks with different PG contents. IPA and water have a lower boiling point than PG and the evaporation of the solvent is relatively fast. The evaporation is fastest at the edge due to the dependence of evaporation rate on surface curvature, leading to particles at the edge are separated out of solvent with large size and deposit firstly on the membrane along with the solvent evaporation, forming a classic coffee ring pattern [32] and larger holes at the center. However, the high boiling point (188.20 °C) of PG slows ink evaporation and the contact line [32] moves slowly with the shrink of the droplet and inside particles immigrate at the same time, forming a compact multilayer structure with smaller size.

The surfaces of the catalyst layers were examined, and the corresponding SEM images are given in Fig. 5. As can be seen in Fig. 5a, the surface is smooth and no obvious cracks can be observed with the PG content of 5 wt%. The CLs made from ink with PG contents of 10 wt% show cracks with I-shape and Y-shape on surface. When the PG content is 30 wt%, increased density of cracks can be seen in Fig. 5c. There is no consensus in the current literature about the mechanism of the crack formation depending on the solvent types [33-36]. In this study, the cracks over the catalyst surface may be caused by different drying stress due to the dense catalyst-ionomer aggregates in ink containing high PG content as shown in Fig. 3e [36]. Additionally, the hydrophobicity of the cathode catalyst layer was also analyzed according to the average static contact angle, and the results are present in the Fig. 5a–c. Contact angle values of all samples exceed 90 ° implying that these surfaces are all hydrophobic. Furthermore, the contact angle decreases significantly as the amount of PG in the ink decreases, i.e. higher PG content in catalyst ink enhances the hydrophobicity of the cathode catalyst layer. Interestingly, the CL at 30% PG is exceptionally hydrophobic. Unfortunately, the straightforward explanation for the difference in hydrophobic of PG-based CL is missing according to our knowledge. Possible reason is that microstructures of CL surfaces vary due to drop size and line spacing/dimensions. As shown in Fig. S5, the morphology of printed lines is quite different as PG content varies. The lines are more separated and line width decreased from (417 ± 43) μm to (267 ± 37) μm and (206 ± 33) μm as the PG content increases due to the decreased size of dried drops in Fig. 4a–c. Therefore, CL surfaces with different roughness may be formed after printing dozens of layers, which in turn affects its hydrophobicity according to the Cassie-Baxter model [37].

Detailed information on the distribution of ionomer and Pt/C within the CL is obtained using AFM as shown in Fig. 6. Specifically, Fig. 6d–f illustrate the ionomer coverage within the CL at various PG contents, corresponding analysis are seen in Fig. 6g–i and calculated values are summarized in Table 1. The areas that appear dark indicate no electronic conductivity and are assumed to be ionomer, while the bright regions indicating high electronic conductivity suggesting the presence of Pt/C catalysts. An increase in PG content from 5 wt% to 30 wt% results in a gradual decline in ionomer coverage of the catalyst from 71% to 56%, implying lower capacity of transporting proton (thicker ionomer layer) as PG content increases. This may be attributed to the fact that ink with low PG content is beneficial for the formation of free ionomer with reduced agglomeration, as depicted in Fig. 3b. Thus, a more uniform and continuous distribution of ionomers can develop within the catalyst layer (CL) [11], promoting increased ionomer coverage and proton transfer path. In conclusion, uniformity and continuity of ionomer distribution are best with the PG content of 5 wt%.

The effects of solvents on the CL microstructure are further revealed by characterizing the cross-sectional structure of CLs by SEM in Fig. 7. Based on the data, the thicknesses of catalyst layers of CL-05P, CL-10P and CL-30P correspond to (2.92±0.18) μm, (2.63±0.14) μm and (2.23 ±0.12) μm, respectively, corresponding to porosities of 52.10%, 46.81% and 37.27%. The whole catalyst layer was made up of stacked dried drops composed of catalyst-ionomer particles. The microstructure of the CL is dense when the catalyst-ionomer particles (see Fig. 3e) and dried drops (see Fig. 4c) are compact [11]. It can be concluded that the CLs printed using ink with 5 wt% PG exhibits highest porosity and thickness, which can be linked to the less agglomerated catalyst-ionomer particles in Fig. 3c and the large size of the dried drop with holes at center in Fig. 4a.

The influence of PG content on the PEMFC performance is shown in Fig. 8. Fig. 8a and b shows polarization curves recorded at the relative humidity of 80% and 50%. Apparently, the OCV of CL-05P is higher than

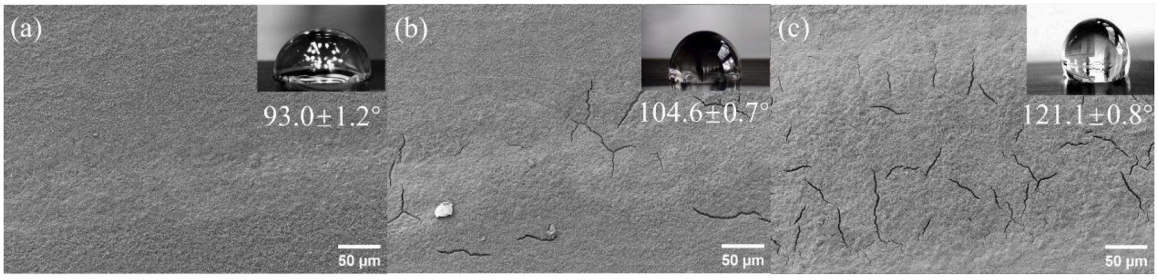

Fig. 5. SEM images of the surface of catalyst layers printed by inks with different PG contents of (a) 5 wt%, (b) 10 wt% and (c) 30 wt%. The insets show contact angle measurements of these surfaces.

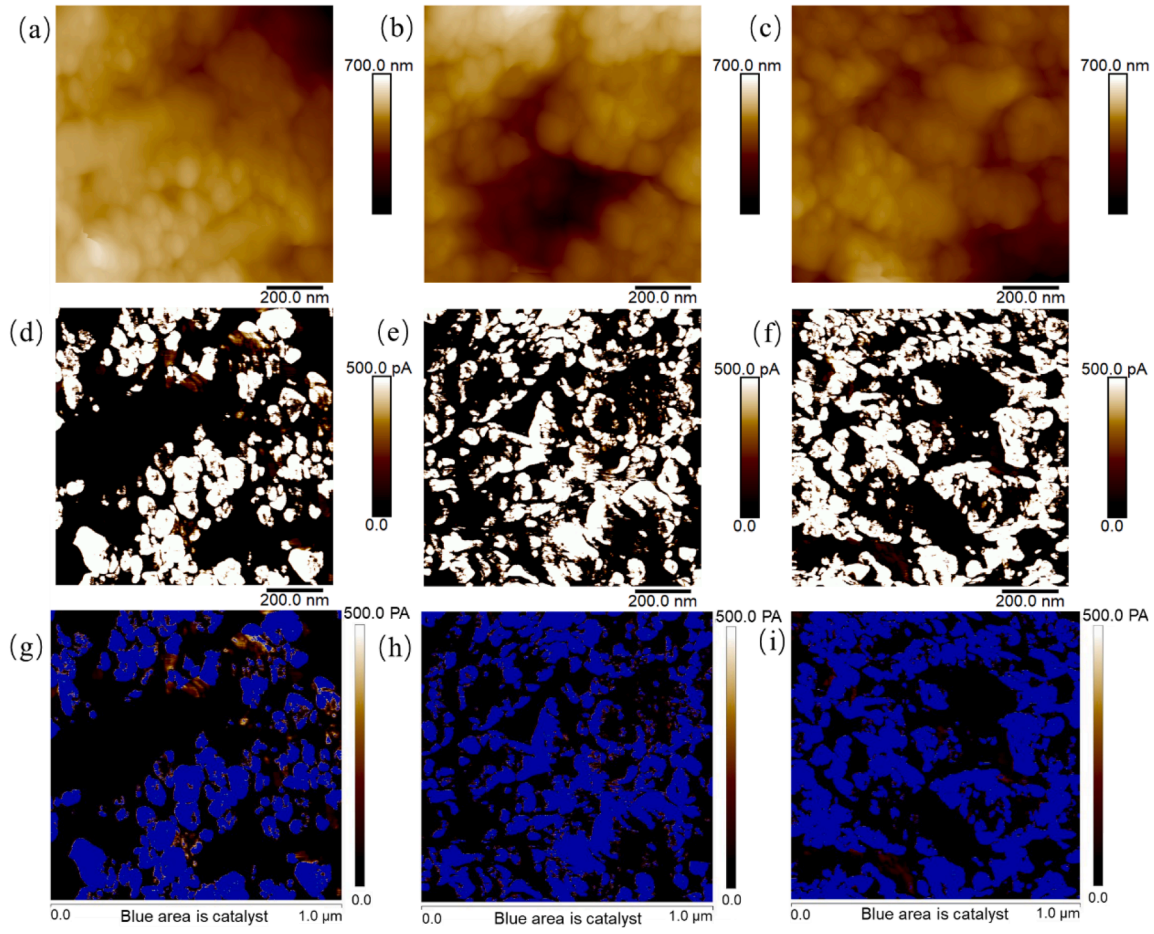

Fig. 6. AFM analysis of CLs prepared by inks with different PG contents (a,d,g) 5 wt%, (b,e,h) 10 wt% and (c,f,i) 30 wt%. (a-c) Morphology images of cross-sectional CLs. (d-f) Corresponding height electrical conductivity measurements (TUNA current) and (g-i) analysis for ionomer coverage by Nanoscope analysis. The ionomer is marked in black, whereas Pt/C is marked in blue.

Table 1
Physical parameters of drop and fabricated cathode layers with different PG contents.

Sample	Drop properties	Catalyst layer properties			
	Feret's diameter of the droplet / µm	Thickness / µm	Porosity /%	Contact angle / °	Ionomer coverage /%
CL-05P	62±6	2.92±0.18	52.10	93.0 ± 1.2	71
CL-10P	57±6	2.63±0.14	46.81	104.6 ± 0.7	64
CL-30P	47±8	2.23±0.12	37.27	121.1 ± 0.8	56

CL-10P and CL-30P, which is related to the decrease of hydrogen crossover at low PG content (see Fig. S9a in the supporting information). Lowest PG content of 5 wt% in ink leads to highest performance with the peak power density of 0.486 W cm^{-2} and performances decrease with increasing PG content in the entire current density range. A drop of peak power density by 30.66% is observed when the PG content is 30 wt%. These general trends are also observed when the relative humidity is decreased to 50%. To analyze the performance losses in more detail, EIS spectra were measured for three electrodes at 0.5 A cm^{-2} with different humidities as shown in Fig. 8c and d as well as in Fig. S6 (supporting information) and Table 2. The intercept on the real axis at the high-frequency region is related to the total ohmic resistance (R_Ω). The diameter of the first and second semicircle illustrates the charge transfer resistance (R_{ct}) and mass transport resistance (R_{mt}), which appears at high current densities and dominates as current increases. The ohmic

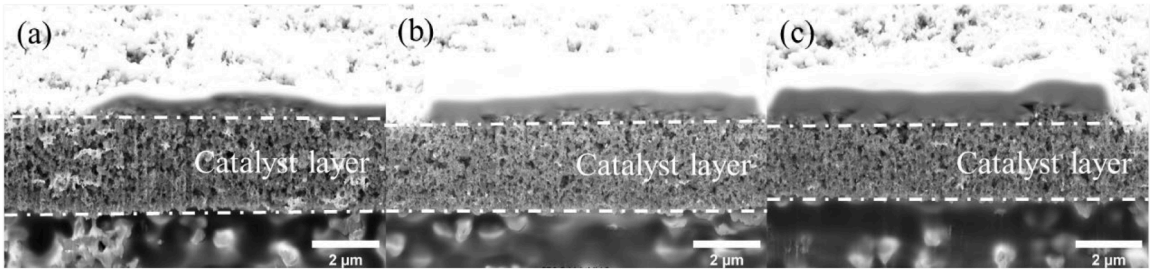

Fig. 7. Cross-sectional FIB-SEM images of the catalyst layers prepared with ink containing PG of (a) 5 wt%, (b) 10 wt% and (c) 30 wt%.

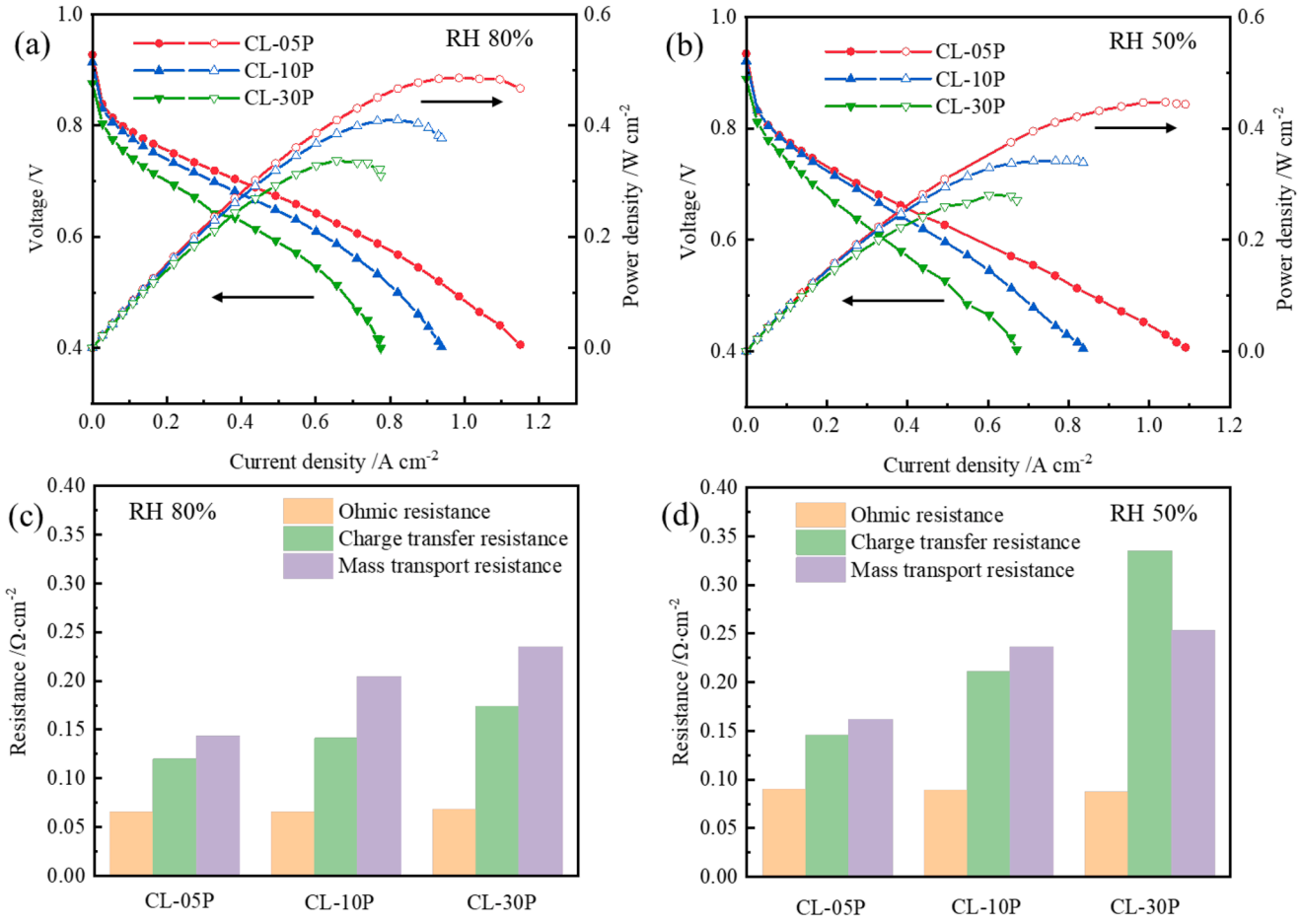

Fig. 8. Effect of PG content on electrochemical properties. H_2/Air polarization and power density curves for the three designed CLs at humidity of (a) 80% and (b) 50%, and resistances determined from EIS data (Fig. S6 in the supporting information) recorded at operating temperature of 80 °C, back pressure of 1.5/1.5 bar (absolute pressure) and flow rate of 0.2/0.4 L min^{-1} at anode and cathode side at humidity of (c) 80% and (d) 50%.

Table 2
Summary of electrochemical results for all inkjet-printed catalyst layers.

	Maximum power density /W cm^{-2}	Current density at 0.6 V /A cm^{-2}	Voltage at 0.6 A cm^{-2} /V	HFR* /Ω cm^2	R_{ct}* /Ω cm^2	R_{mt}* /Ω cm^2	RH /%	ECSA* /m^2 g_{Pt}^{-1}
CL-05P	0.486	0.732	0.643	0.065	0.120	0.143	80	33.26
CL-10P	0.410	0.622	0.609	0.065	0.141	0.205	80	29.71
CL-30P	0.337	0.472	0.545	0.068	0.174	0.235	80	15.74
CL-05P	0.447	0.573	0.591	0.090	0.145	0.162	50	–
CL-10P	0.342	0.484	0.546	0.089	0.211	0.236	50	–
CL-30P	0.280	0.344	0.466	0.087	0.335	0.253	50	–

* All resistances are measured at 0.5 A cm^{-2} and ECSA values are collected at 100% RH. In addition, the error due to fitting via Zahner Software is less than 10% for all reported resistance values.

resistance of CLs prepared with different inks are basically the same at RH of 80% and 50% because of the same membrane, catalyst and GDL. The values of R_{ct} varied from 0.120 to 0.141 and 0.174 Ω cm^2 with the alteration of PG contents and the respective values of R_{mt} for CL-05P, CL-10P and CL-30P are 0.143, 0.205 and 0.235 Ω cm^2 at RH of 80%. As expected, when the humidity is reduced to 50%, $R_Ω$ increases for each sample due to the dehydration of the membrane and ionomer related to the increase of proton transfer resistance. The tendency of the resistance depending on PG contents in the ink was same even though the humidity is lowered: R_{ct} (CL-05P)<R_{ct} (CL-10P)<R_{ct} (CL-30P) and R_{mt} (CL-05P)< R_{mt} (CL-10P)<R_{mt} (CL-30P). Generally, the CL printed using ink with lowest PG content (CL-05P) exhibits the lowest charge transfer resistance possibly attributed to the larger contact area at triple-phase boundary caused by weakened agglomeration behavior (see Fig. 3c), which is beneficial to ORR reactions and leads to less voltage loss at low current density [29]. The lowest mass transport resistance of CL-05P is mainly attributed to more porous structure (Fig. 7c) caused by larger dried drops compared with other microstructures. Although CL-30P is

more hydrophobic according to Fig. 5c, voltage loss at high current density has not been mitigated compared with the effect of porosity.

The ECSA of the cathode electrodes as a function of PG concentration is displayed in Fig. 9a, with the corresponding cyclic voltammetry measurements shown in Fig. S7d (supporting information). Apparently, ECSA decreases non-linearly with increasing PG content, showing a slight reduction of 10.67% for CL printed with 10 wt% PG but a significant drop of 52.68% when the ink contains 30 wt% PG compared with CL-05P A reason could be the more compact shape of Pt/C-ionomer particles with high PG content (see Fig. 3c–e) which leads to less exposed reaction area on Pt surface. The proton transport resistances (R_{H+}) determined using EIS in H_2/N_2 atmospheres under different relative humidities are depicted in Fig. 9b (see also in Fig. S7a–c, supporting information). As expected, R_{H+}values decrease with increasing humidity due to higher hydration of the ionomer. Specifically, the R_{H+} of CL-30P consistently exceeds that of both the CL-05P and CL-10P at different humidities and the gap in R_{H+} values among these CLs tends to diminish progressively as the humidity increases. This occurs because free water itself can form a network that helps proton conduction at highly humidified conditions [38]. The decreased $R_{H+}$of CL-05P as compared to other CLs allows for the high proton conductivity, which is ascribed to the higher ionomer coverage, and uniform and continuous ionomer distribution in the CL obtained by AFM in Fig. 6d–f. Above decreased $R_{H+}$of CL-05P plays a dominant role in reduction of voltage losses in ohmic region of the IV curve in Fig. 8a and b because the ohmic resistances (R_Ω) are almost same at the same humidity [39].

In addition, another high-boiling point solvent (EG) was investigated and compared with results obtained using PG. The electrochemical characterization is presented in Fig. 10a and b. It is clear that PG content should be kept low to avoid compromising MEA performance. Thus, ink containing only 5 wt% of EG was used to prepare a cathode catalyst layer labelled as CL-05E. Similarly, the hydrogen crossover of CL-05P is lower than that of CL-05E (Fig. S9a), leading to a higher OCV of CL-05P compared to CL-05E. The MEA with CL-05E yields a maximum power density of 0.424 W cm^{-2} at 80% RH and 0.378 W cm^{-2} at 50% RH, lower than CL-05P with value of 0.486 W cm^{-2} (80% RH) and 0.447 W cm^{-2} (50% RH), respectively. The reduced electrochemical performance of MEA containing EG compared to PG is ascribed mainly to substantial increases of mass transport resistance in Fig. 10c and d and Table S4. We speculate that the reason might be the different porosity in the CL. Cyclic voltammograms of CL-05E are provided in Fig. S9b (supporting information) showing a decrease of ECSA by 27% compared to the CL-05P (also see in Table S4). It can be concluded that ink containing PG is more conducive to the preparation of catalyst layer with higher electrochemical performance compared with EG. The provided results show how the concentration and type of high boiling point solvents influence CL performance. However, the durability of the CL is also necessary to be discussed especially in context of demanding heavy-duty applications [40]. According to literature, the type of solvent indeed affects the stability of the prepared CLs [10]. The voltage loss of CLs at 1 A cm^{-2} made by aqueous solvent like 2-propanol/water and 1-propanol/water is ~80 mV after 30k voltage cycling tests, while for CLs prepared by non-aqueous slovent like 1,2-butanediol and ethylene glycol a lower voltage loss of 35 mV is reported. Jong-Hyeok Park et al. [41] found that CLs with smaller aggregates of the ionomer, thinner ionomer layer surrounding electrocatalyst and the crack-free surface were formed based on EG-based solvent, enhancing the stability of the CLs after 30k voltage cycles compared with CLs prepared by water-based solvent. In our study, ionomer network and cracks on CL surface depend on the PG content in the ink. However, articles discussing the stability of the catalyst layer prepared with PG-based solvent could not be identified. Thus, in future studies the focus should be extended to investigating the impact of solvent and the resulting catalyst layer structures on PEMFC durability which is main concern in context of heavy-duty applications.

5. Conclusions

In this study, the effects of high boiling point solvents on the printing process and on the performance of PEM fuel cells with low Pt loading (0.1 mg cm^{-2}) were investigated. It is found that adding high boiling point solvents (EG or PG) as additives can greatly reduce time to print CLs compared with standard ink (only IPA/water as solvent) due to faster ink deposition and less frequent cleaning of blocked printing nozzle. AFM and microscopy images indicate that the difference in solvent evaporating conditions during drying process caused by inks with different PG content has great impact on CL microstructure and properties such as catalyst-ionomer cluster, leading to different proton transport resistance, mass transport resistance and ECSA. Moreover, PG content affects the hydrophobicity of the CL. Generally, high PG content is detrimental regarding MEA performance. For the CL prepared by ink with 30 wt% PG, a reduction of ECSA by 52.68% was observed along with a substantial reduction of CL porosity by 28% and increase of proton transport resistance leading to an overall drop of PEMFC peak performance by 31% at humidity of 80%. The type of high-boiling point solvent is also relevant as demonstrated by comparing the electrochemical performance of PG and EG, with the latter causing greater

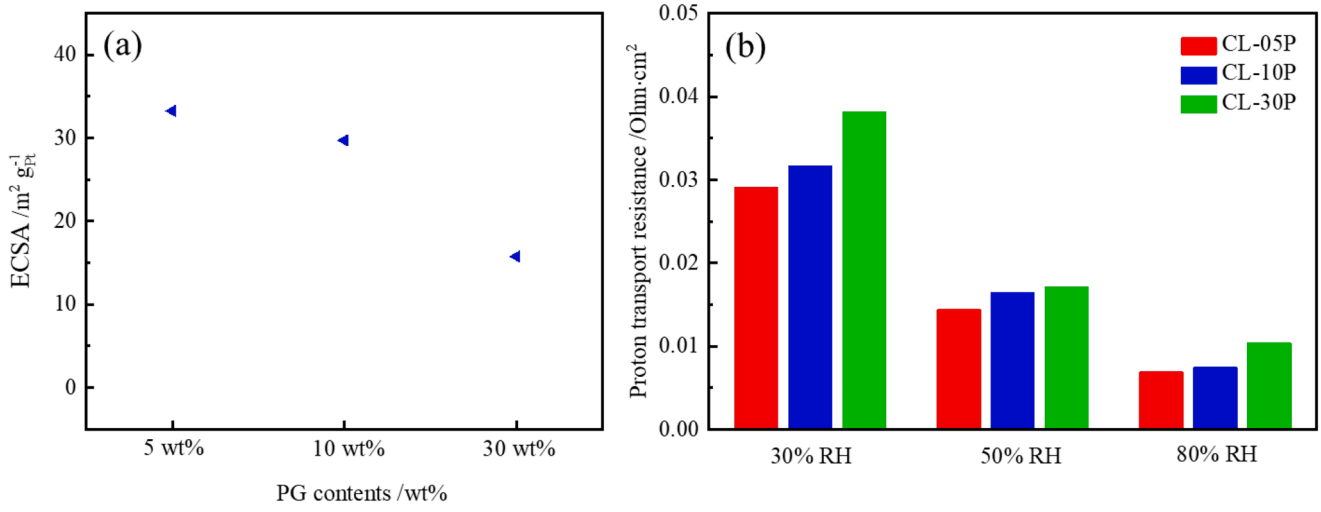

Fig. 9. (a) ECSA values for three designed CLs calculated from cyclic voltammetry curves according to Fig. S7d (supporting information); (b) Proton transport resistances of different catalyst layers determined from EIS spectra recorded at different humidities, 80 °C, 1.5/1.5 bar, and flow rate of 0.1/0.1 L min^{-1} H_2/N_2 based on Fig. S7 and Table S3 (supporting information).

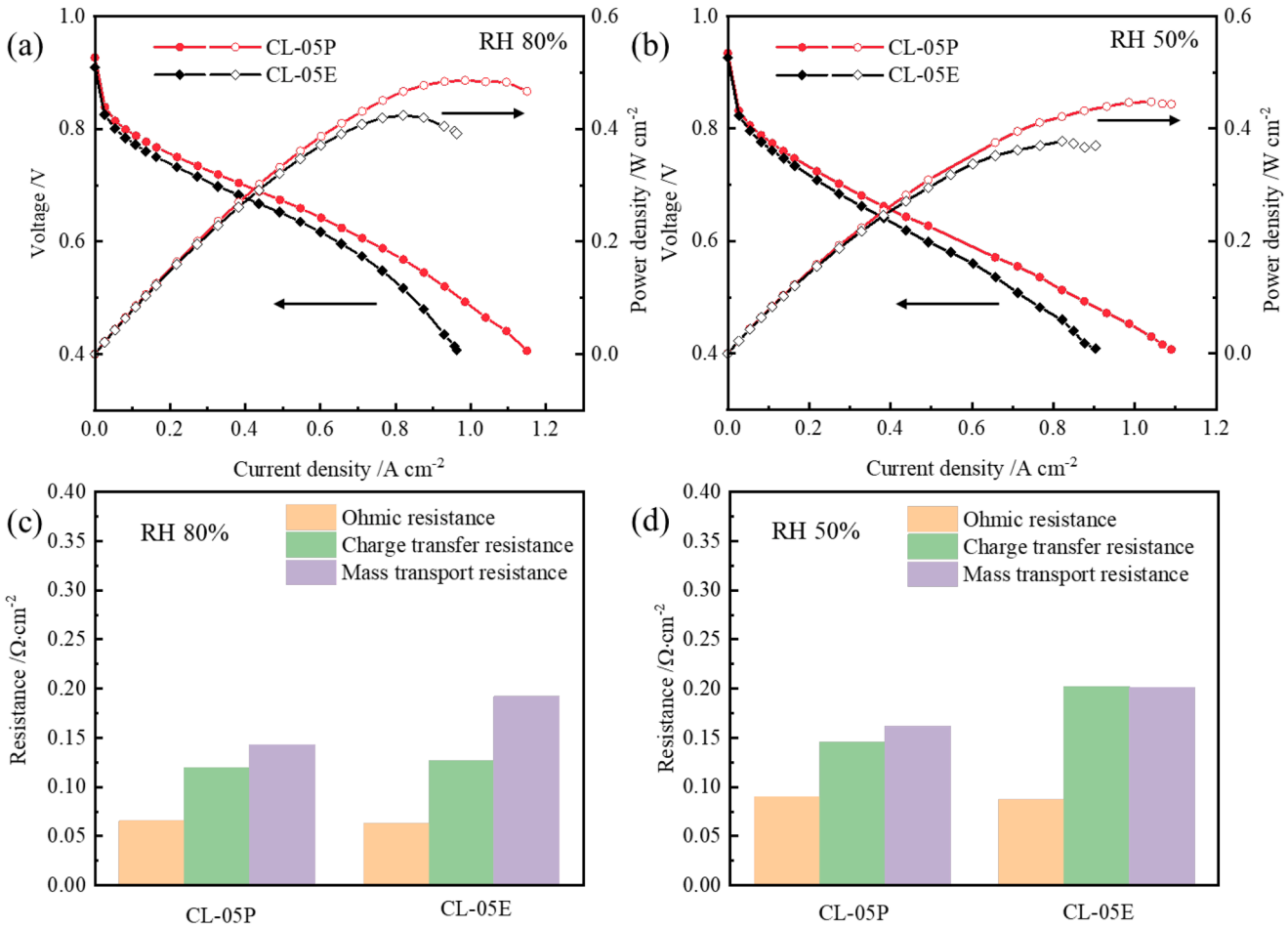

Fig. 10. H_2/Air polarization and power density curves for CL prepared with PG and EG at different humidity of (a) 80% and (b) 50%, and variations of the resistances with different additives, recorded at humidity of (c) 80 wt% according to Fig. S8a (supporting information) and (d) 50 wt% according to Fig. S8b (supporting information), operating temperature of 80 °C, back pressure of 1.5/1.5 bar (absolute pressure) and flow rate of 0.2/0.4 L min^{-1} at anode and cathode.

performance loss. These findings link the microstructure of the CL to the physical properties of ink composition and provide novel insights into the solvent selection of inkjet-printed CLs. Even though the printing time of CL decreases with increasing PG concentrations, only low PG concentrations should be considered for MEA preparation to avoid strong performance losses. However, total omission of high-boiling point solvents makes the IJP process unreliable and selection of proper solvent composition is key challenge to allow wide-spread allocation of IJP in fuel cell technologies.

CRediT authorship contribution statement

Qingying Zhao: Conceptualization, Investigation, Methodology, Data curation, Formal analysis, Validation, Visualization, Writing – original draft. **Tobias Morawietz:** Formal analysis, Methodology, Writing – review & editing. **Pawel Gazdzicki:** Supervision, Writing – review & editing, Funding acquisition. **K. Andreas Friedrich:** Supervision, Writing – review & editing.

Declaration of competing interest

The authors declare that they have no known competing financial interests or personal relationships that could have appeared to influence the work reported in this paper.

Acknowledgments

Dedicated to Prof. Elena Savinova in recognition of her tireless dedication to electrocatalysis.

This work was financially supported by the DAAD-DLR scholarship. The authors gratefully acknowledge the core facility SRF AMICA (Stuttgart Research Focus Advanced Materials Innovation and Characterization) at the University of Stuttgart for their support & assistance in this work. Their research was supported by the German Research Foundation (DFG, AOBJ: 661806).

The research leading to the results received funding from the Fuel Cells and Hydrogen 2 Joint Undertaking (now Clean Hydrogen Partnership) under Grant Agreement No 875025 (Further-FC). This Joint Undertaking receives support from the European Union's Horizon 2020 Research and Innovation program, Hydrogen Europe and Hydrogen Europe Research.

The authors also thank Siegfried Graf for his efforts in setting up and maintaining the fuel cell test bench.

Supplementary materials

Supplementary material associated with this article can be found, in the online version, at doi:10.1016/j.electacta.2024.145273.

Data availability

Data will be made available on request.

References

[1] Y. Zhou, M.Y. Wu, K. Meng, Y.R. Liu, P. Rao, X. Wu, S.Y. Huang, K. Li, C.W. Zheng, D.X. Wu, P.L. Deng, J. Li, X.l. Tian, Z.Y. Kang, Microscale structure optimization of catalyst layer for comprehensive performance enhancement in proton exchange membrane fuel cell, Energy 301 (2024) 131738, https://doi.org/10.1016/j.energy.2024.131738.

[2] J. Sharma, X. Lyu, T. Reshetenko, G. Polizos, K. Livingston, J. Li, D.L. Wood, A. Serov, Catalyst layer formulations for slot-die coating of PEM fuel cell electrodes, Int. J. Hydrog. Energy 47 (2022) 35838–35850, https://doi.org/10.1016/j.ijhydene.2022.08.157.

[3] H. Su, T.-C. Jao, O. Barron, B.G. Pollet, S. Pasupathi, Low platinum loading for high temperature proton exchange membrane fuel cell developed by ultrasonic spray coating technique, J. Power Source. 267 (2014) 155–159, https://doi.org/10.1016/j.jpowsour.2014.05.086.

[4] L.F. Arenas, G. Hadjigeorgiou, S. Jones, N. van Dijk, D. Hodgson, A. Cruden, C. Ponce de León, Effect of airbrush type on sprayed platinum and platinum-cobalt catalyst inks: benchmarking as PEMFC and performance in an electrochemical hydrogen pump, Int. J. Hydrog. Energy 45 (2020) 27392–27403, https://doi.org/10.1016/j.ijhydene.2020.06.292.

[5] L. Ney, J. Hog, R. Singh, N. Göttlicher, P. Schneider, S. Tepner, M. Klingele, R. Keding, F. Clement, U. Groos, Challenges of fabricating catalyst layers for PEM fuel cells using flatbed screen printing, J. Coat. Technol. Res. 20 (2023) 73–86, https://doi.org/10.1007/s11998-022-00710-1.

[6] K. Talukdar, T. Morawietz, P. Sarkezi-Selsky, K. Yezerska, O. Sergeev, J.-F. Heger, T. Jahnke, P. Gazdzicki, K.A. Friedrich, Exploring critical parameters of electrode fabrication in polymer electrolyte membrane fuel cells, J. Power Source. 540 (2022) 231638, https://doi.org/10.1016/j.jpowsour.2022.231638.

[7] C.A. Gomes Bezerra, L.J. Deiner, G. Tremiliosi-Filho, Unexpected performance of inkjet-printed membrane electrode assemblies for proton exchange membrane fuel cells, Adv. Eng. Mater. 21 (2019) 1900703, https://doi.org/10.1002/adem.201900703.

[8] A. Willert, F.Z. Tabary, T. Zubkova, P.E. Santangelo, M. Romagnoli, R.R. Baumann, Multilayer additive manufacturing of catalyst-coated membranes for polymer electrolyte membrane fuel cells by inkjet printing, Int. J. Hydrog. Energy 47 (2022) 20973–20986, https://doi.org/10.1016/j.ijhydene.2022.04.197.

[9] B.G. Pollet, S.S. Kocha, I. Staffell, Current status of automotive fuel cells for sustainable transport, Curr. Opin. Electrochem. 16 (2019) 90–95, https://doi.org/10.1016/j.coelec.2019.04.021.

[10] C. Lei, F. Yang, N. Macauley, M. Spinetta, G. Purdy, J. Jankovic, D.A. Cullen, K. L. More, Y.S. Kim, H. Xu, Impact of catalyst ink dispersing solvent on PEM fuel cell performance and durability, J. Electrochem. Soc. 168 (2021) 44517, https://doi.org/10.1149/1945-7111/abf2b0.

[11] H. Ren, X. Meng, Y. Lin, Z. Shao, Microstructure formation mechanism of catalyst layer and its effect on fuel cell performance: effect of dispersion medium composition, J. Energy Chem. 73 (2022) 588–598, https://doi.org/10.1016/j.jechem.2022.06.034.

[12] Q. Gong, C. Li, Y. Liu, J. Ilavsky, F. Guo, X. Cheng, J. Xie, Effects of ink formulation on construction of catalyst layers for high-performance polymer electrolyte membrane fuel cells, ACS Appl. Mater. Interface. 13 (2021) 37004–37013, https://doi.org/10.1021/acsami.1c06711.

[13] K.B. Hatzell, M.B. Dixit, S.A. Berlinger, A.Z. Weber, Understanding inks for porous-electrode formation, J. Mater. Chem. A 5 (2017) 20527–20533, https://doi.org/10.1039/C7TA07255D.

[14] R. Bernasconi, S. Brovelli, P. Viviani, M. Soldo, D. Giusti, L. Magagnin, Piezoelectric drop-on-demand inkjet printing of high-viscosity inks, Adv. Eng. Mater. 24 (2022), https://doi.org/10.1002/adem.202100733.

[15] S. Shukla, D. Stanier, M.S. Saha, B. Zahiri, M. Tam, J. Stumper, M. Secanell, Characterization of inkjet printed electrodes with improved porosity, ECS Trans. 77 (2017) 1453–1463, https://doi.org/10.1149/07711.1453ecst.

[16] M.B. Sassin, Y. Garsany, B.D. Gould, K.E. Swider-Lyons, Fabrication method for laboratory-scale high-performance membrane electrode assemblies for fuel cells, Anal. Chem. 89 (2017) 511–518, https://doi.org/10.1021/acs.analchem.6b03005.

[17] N. Hasegawa, A. Kamiya, T. Matsunaga, N. Kitano, M. Harada, Analysis of crack formation during fuel cell catalyst ink drying process. Reduction of catalyst layer cracking by addition of high boiling point solvent, Colloid. Surf. A: Physicochem. Eng. Asp. 628 (2021) 127153, https://doi.org/10.1016/j.colsurfa.2021.127153.

[18] A. Li, M. Han, S.H. Chan, N. Nguyen, Effects of hydrophobicity of the cathode catalyst layer on the performance of a PEM fuel cell, Electrochim. Acta 55 (2010) 2706–2711, https://doi.org/10.1016/j.electacta.2009.12.048.

[19] Q. Wang, M. Eikerling, D. Song, Z. Liu, Functionally graded cathode catalyst layers for polymer electrolyte fuel cells: I. Theoretical modeling, J. Electrochem. Soc. 151 (2004) A950, https://doi.org/10.1149/1.1753580.

[20] S. Shukla, K. Domican, K. Karan, S. Bhattacharjee, M. Secanell, Analysis of low platinum loading thin polymer electrolyte fuel cell electrodes prepared by inkjet printing, Electrochim. Acta 156 (2015) 289–300, https://doi.org/10.1016/j.electacta.2015.01.028.

[21] H.K. Cader, G.A. Rance, M.R. Alexander, A.D. Gonçalves, C.J. Roberts, C.J. Tuck, R. D. Wildman, Water-based 3D inkjet printing of an oral pharmaceutical dosage form, Int. J. Pharm. 564 (2019) 359–368, https://doi.org/10.1016/j.ijpharm.2019.04.026.

[22] D.H.A.T. Gunasekera, S. Kuek, D. Hasanaj, Y. He, C. Tuck, A.K. Croft, R. D. Wildman, Three dimensional ink-jet printing of biomaterials using ionic liquids and co-solvents, Faraday Discuss 190 (2016) 509–523, https://doi.org/10.1039/c5fd00219b.

[23] S.D. Hoath, Fundamentals of Inkjet printing: the Science of Inkjet and Droplets, John Wiley & Sons, 2016.

[24] Q. Zhang, M. Schulze, P. Gazdzicki, K.A. Friedrich, Comparison of different performance recovery procedures for polymer electrolyte membrane fuel cells, Appl. Energy 302 (2021) 117490, https://doi.org/10.1016/j.apenergy.2021.117490.

[25] G. Tsotridis, A. Pilenga, G. De Marco, T. Malkow, EU Harmonised Test Protocols for PEMFC MEA Testing in Single Cell Configuration for Automotive Applications, Publications Office of the European Union, Luxembourg, 2015, https://doi.org/10.2790/54653.

[26] V.R. Kevin, R. Cooper, J.M. Fenton, H.R. Kunz, Experimental Methods and Data Analyses for Polymer Electrolyte Fuel Cells, Scribner Associates, 2005.

[27] A.D. Modestov, A.V. Kapustin, V.B. Avakov, I.K. Landgraf, M.R. Tarasevich, Cathode catalyst layers with ionomer to carbon mass ratios in the range 0–2 studied by electrochemical impedance spectroscopy, cyclic voltammetry, and performance measurements, J. Power Source. 272 (2014) 735–742, https://doi.org/10.1016/j.jpowsour.2014.08.113.

[28] S. Dou, L. Hao, H. Liu, Effects of carbon aggregates and ionomer distribution on the performance of PEM fuel cell catalyst layer: a pore-scale study, Renew. Energy 217 (2023) 119254, https://doi.org/10.1016/j.renene.2023.119254.

[29] T.H. Kim, J.Y. Yi, C.Y. Jung, E. Jeong, S.C. Yi, Solvent effect on the Nafion agglomerate morphology in the catalyst layer of the proton exchange membrane fuel cells, Int. J. Hydrog. Energy 42 (2017) 478–485, https://doi.org/10.1016/j.ijhydene.2016.12.015.

[30] J.H. Jong Y. J, G. Doo, J. Jung, S. Choi, D.H. Lee, D.W. Lee, J. Kwen, W. Jo, C. Bae, H.T. Kim, Tailoring catalyst layer structures for anion exchange membrane fuel cells by controlling the size of ionomer aggregates in dispersion, Chem. Eng. J. 427 (2022) 131737, https://doi.org/10.1016/j.cej.2021.131737.

[31] W.H. WALTON, Feret's Statistical diameter as a measure of particle size, Nature 4113 (1948) 329–330, https://doi.org/10.1038/162329b0.

[32] A. Kaliyaraj Selva Kumar, Y. Zhang, D. Li, R.G. Compton, A mini-review: how reliable is the drop casting technique? Electrochem. Commun. 121 (2020) 106867 https://doi.org/10.1016/j.elecom.2020.106867.

[33] S. Woo, S. Lee, A.Z. Taning, T.H. Yang, S.H. Park, S.D. Yim, Current understanding of catalyst/ionomer interfacial structure and phenomena affecting the oxygen reduction reaction in cathode catalyst layers of proton exchange membrane fuel cells, Curr. Opin. Electrochem. 21 (2020) 289–296, https://doi.org/10.1016/j.coelec.2020.03.006.

[34] D.C. Huang, P.J. Yu, F.J. Liu, S.L. Huang, K.L. Hsueh, Y.C. Chen, C.H. Wu, W. C. Chang, F.H. Tsau, Effect of dispersion solvent in catalyst ink on proton exchange membrane fuel cell performance, Int. J. Electrochem. Sci. 7 (2011) 2551–2565, https://doi.org/10.1016/S1452-3981(23)18202-2.

[35] M. Yamamura, H. Ono, T. Uchinomiya, Y. Mawatari, H. Kage, Multiple crack nucleation in drying nanoparticle-polymer coatings, Colloid. Surf. A: Physicochem. Eng. Asp. 342 (2009) 65–69, https://doi.org/10.1016/j.colsurfa.2009.04.008.

[36] N. Kumano, K. Kudo, A. Suda, Y. Akimoto, M. Ishii, H. Nakamura, Controlling cracking formation in fuel cell catalyst layers, J. Power Source. 419 (2019) 219–228, https://doi.org/10.1016/j.jpowsour.2019.02.058.

[37] M. Sonal, Y. Fan, C.J. Cornelius, Carbon-Ionomer Nanocomposite Wetting Properties: the Role of Ionomer Composition and Surface Roughness, Int. J. Mater. Sci. Appl. 4 (2) (2015) 69–76, https://doi.org/10.11648/j.ijmsa.20150402.11.

[38] Y. Liu, C. Ji, W. Gu, D.R. Baker, J. Jorne, H.A. Gasteiger, Proton conduction in PEM fuel cell cathodes: effects of electrode thickness and ionomer equivalent weight, J. Electrochem. Soc. 157 (2010) B1154, https://doi.org/10.1149/1.3435323.

[39] F. Du, T.A. Dao, P.V.J. Peitl, A. Bauer, K. Preuss, A.M. Bonastre, J. Sharman, G. Spikes, M. Perchthaler, T.J. Schmidt, Effects of PEMFC operational history under dry/wet conditions on additional voltage losses due to ionomer migration, J. Electrochem. Soc. 167 (2020) 144513.

[40] C.S. Gittleman, H.F. Jia, E.D. Castro, C.R.I. Chisholm, Y.S. Kim, Proton conductors for heavy-duty vehicle fuel cells, Joule 7 (2021) 1660–1677, https://doi.org/10.1016/j.joule.2021.05.016.

[41] J.H. Park, M.S. Shin, J.S. Park, Effect of dispersing solvents for ionomers on the performance and durability of catalyst layers in proton exchange membrane fuel cells, Electrochim. Acta 391 (2021) 138971, https://doi.org/10.1016/j.electacta.2021.138971.